Monthly Notices
of the
ROYAL ASTRONOMICAL SOCIETY

MNRAS **441,** 2845–2854 (2014) doi:10.1093/mnras/stu725

Analysis of 1SWASP J140747.93−394542.6 eclipse fine-structure: hints of exomoons

T. I. M. van Werkhoven,[1]★ M. A. Kenworthy[1] and E. E. Mamajek[2]

[1]*Leiden Observatory, Leiden University, PO Box 9513, NL-2300 RA Leiden, the Netherlands*
[2]*Department of Physics and Astronomy, University of Rochester, Rochester, NY 14627-0171, USA*

Accepted 2014 April 9. Received 2014 April 8; in original form 2014 January 31

ABSTRACT

A recently discovered $V = 12.3$ mag K5 pre-main-sequence star in the SuperWASP (Super Wide Angle Search for Planets) data base shows a peculiar light curve with a highly structured eclipse pattern covering a timespan of at least 54 d with maximum dimming of at least 3.3 mag. The central eclipse is surrounded by two 1 mag eclipses at ±12 and ±26 d. The authors speculate that the star is eclipsed by a substellar companion with an extended and highly structured ring system. To investigate the nightly light-curve structure and to confirm the multiple-ring hypothesis, we have carried out a calibrated reduction of the SuperWASP data, removing both systematic errors and periodic stellar variability. We count at least 24 inflection points on ingress and 16 on egress, consistent with the presence of at least 24 rings in this disc. By measuring the light-curve slope, we find implied speeds for the eclipsing object that are incompatible with a closed Kepler orbit with $P = 2.3$ yr. We propose several scenarios that could give rise to such light-curve slopes and find that azimuthal ring structure (analogous to 'spokes' seen in Saturn's rings) can account for the observed light curve. The highly structured ring system also implies the presence of exomoons orbiting the secondary companion.

Key words: planets and satellites: formation – planets and satellites: rings – binaries: eclipsing – planetary systems – stars: individual: 1SWASP J140747.93−394542.6 (ASAS J140748−3945.7).

1 INTRODUCTION

Mamajek et al. (2012) discovered the peculiar light curve of a young ∼16 Myr, 0.9 $M_\odot$, $V = 12.3$ mag K5 star (1SWASP J140747.93−394542.6 = ASAS J140748−3945.7, hereafter J1407) in *The Super Wide Angle Search for Planets* (henceforth SuperWASP) data base (Butters et al. 2010). The light curve as observed by SuperWASP shows a deep >3.3 mag eclipse with two pairs of eclipses occurring symmetrically 12 and 26 d before and after the eclipse mid-point, parts of which are confirmed by the lower cadence *All Sky Automated Survey* data. Light-curve variability induced by extended disc eclipses is not unique, as seen in the stars EE Cep (Mikolajewski & Graczyk 1999) and ϵ Aurigae (Guinan & Dewarf 2002) which show related complex asymmetric eclipses caused by discs orbiting the primary star.

The authors propose and reject several explanations for these observations. An eclipse by an isolated (sub)stellar companion alone would not yield a >95 per cent dimming, nor does it explain the eclipse fine-structure seen in the nightly photometry. An eclipsing binary where a red giant eclipses a fainter, bluer star is rejected on spectroscopic grounds; there is no evidence for a giant in J1407, nor would it give rise to the structure observed in the eclipse weeks before and after the primary eclipse. A disc orbiting an old stellar remnant companion obscuring the primary is unlikely because the system is very young. A circumbinary or circumstellar disc obscuring the primary is unlikely because there is no excess infrared observed at J1407 indicative of such a thick disc. Additionally, the minimum orbital period of 2.33 yr they find is incompatible with this scenario. A disc orbiting J1407 obscuring the star light due to the relative motion between us and J1407 would yield a one-time eclipsing event, but is disregarded because it requires a very thin disc (aspect ratio height over radius $\sim 10^{-8}$) and it does not explain the symmetric dimming around the central minimum. Finally, a more massive companion obscured by a disc orbiting it is unlikely again due to lack of infrared excess.

The scenario Mamajek et al. (2012) propose involves a circumsecondary or circumplanetary disc, which obscures the primary star, J1407. Based on the absence of a second eclipse, the authors constrain the period $P > 2.33$ yr, yielding an orbital radius greater than 17 au and a circular orbital velocity less than 21.7 km s^{-1} (assuming $m_1 = 0.9\,M_\odot$). They propose a preliminary 4-ring model with a

★ E-mail: werkhoven@strw.leidenuniv.nl

central opaque disc accompanied by three discrete rings with opacities $\tau = 0.5, 0.2, 0.05$. To match the observations, this model has an orbital inclination of 89.°955 and the ring plane is tilted by 13° to the orbital plane.

In this paper, we carry out a new reduction of the SuperWASP data, taking care of systematic inter-CCD differences and additionally remove stellar variability due to the rotation of the star (described in Section 2). We then investigate the nightly fine structure in the photometric signal, focusing specifically on the light-curve slope and its implications for the nature of the eclipsing structure (Sections 4 and 5). We propose several possible scenarios for these findings and conclude with suggestions to better constrain the system in Section 6.

2 DATA REDUCTION

The SuperWASP (Pollacco et al. 2006) observatories are located at the Observatorio del Roque de los Muchachos on La Palma, and at the Sutherland Station of the South African Astronomical Observatory. Both facilities consist of a telescope with eight lenses (Canon 200 mm *f*/1.8), each mounted on a 2048 × 2048-pixel back-illuminated CCD (e2v). Each lens has a field of view of ∼64 deg^2, for a total of ∼482 deg^2 per telescope. The data acquisition cadence is 9 min to 12 min for each camera (Butters et al. 2010).

The SuperWASP data base has coverage of J1407 during the seasons of 2006 through 2008 (depicted in the upper panel of Fig. 1). The star was observed on CCDs 221, 227 and 228. CCDs 227 and 228 have coverage of J1407 during 2006, 2007 and 2008, while CCD 221 only has coverage during the 2007 season. The SuperWASP pipeline provides simple aperture photometry (Kane et al. 2004), as well as automatically reduced flux according to the TAMUZ correction (Cameron et al. 2007; Tamuz, Mazeh & Zucker 2005).

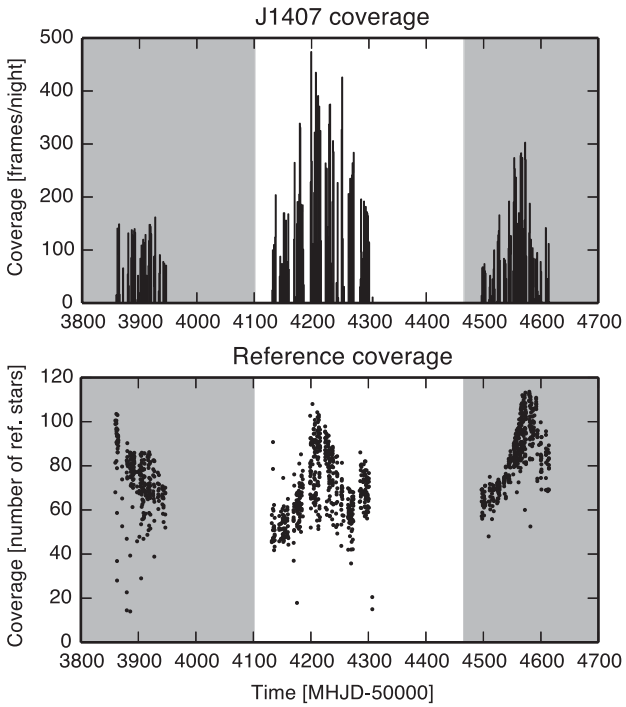

Figure 1. Top: number of SuperWASP observations of J1407, summed for all CCDs. Bottom: number of reference stars co-temporally observed with J1407 for all CCDs, averaged per day. Years 2006 and 2008 are shaded. The eclipse occurred in 2007 around MHJD 54 222.

We find that the automatic correction does not produce optimal photometry for this specific target, which can be expected considering the long and structured eclipse signal this light curve shows, and the star's location at the corner of the field of view of the three cameras.

Because of this variability, we began our reduction with the simple aperture photometry flux instead of using the automatically reduced flux. First, we de-correlated the systematic errors from the light curve by using a selected ensemble of nearby stars to act as a photometric standard, allowing direct comparison of the data from different CCDs (Section 2.1). After de-correlation, we removed the stellar variability from the light curve through phase dispersion minimization (Section 2.2).

2.1 Systematics de-correlation

The multiple CCDs of SuperWASP provide significantly different light curves, as observed by Mamajek et al. (2012) and Norton et al. (2011). To mitigate this effect, we de-correlated systematic errors between the CCDs based on Tamuz et al. (2005) and de-correlation techniques used by *Kepler* (Fraquelli & Thompson 2012, p. 21).[1]

First, we select a set of 388 reference stars in a cone of 20 arcmin centred on J1407 that are also observed by SuperWASP, $R_{\rm all}$. The bottom panel in Fig. 1 shows the number of reference stars co-temporally observed with J1407, summed for all CCDs, averaged per day. Because of temporal gaps in both the target and reference data, we cannot perform a global analysis of a set of reference stars for our target star, and adapted the methods mentioned above to work on a point-by-point basis.

For each CCD separately, we used only reference stars for which at least 25 per cent of the data points are co-temporally observed with J1407, $R_{\rm cotemp}$:

$$R_{\rm cotemp} = \{x \in R_{\rm all} | \#(x_{\rm exp} \cup {\rm tgt}_{\rm exp}) > 0.25\#({\rm tgt})\}. \quad (1)$$

Of this subset, we selected 75 per cent that have a low variance $\sigma_{\rm ref}$ (i.e. quiet stars), defined as the standard deviation of the median-normalized flux

$$\sigma_{\rm ref} = {\rm stddev}(F_{\rm ref})/{\rm median}(F_{\rm ref}). \quad (2)$$

We require photometrically quiet stars to measure the systematics of the cameras. This criterion was chosen to reject the most variable reference stars (see Fig. 2). In this way, we obtained approximately 60–100 suitable reference stars, $R_{\rm quiet}$, per exposure of our target.

$$R_{\rm quiet} = \{x \in R_{\rm cotemp} | \sigma(x/{\rm median}(x)) < \sigma(x/{\rm median}(x))_{75\ {\rm per\ cent}}\}. \quad (3)$$

For this subset of reference stars, we calculated the mean of the median-normalized flux for all exposures co-temporal with our target,

$$F_{\rm decorr}(t) = \sum^{i \in R_{\rm quiet}} F_i(t)/\#(R_{\rm quiet}(t)) \quad \text{for } t \in t_{\rm obs}, \quad (4)$$

where $t_{\rm obs}$ are times at which J1407 was observed. We then divide the flux of J1407 by the thus obtained de-correlation vector $F_{\rm decorr}$ for each CCD.

Using the average of these reference stars suppresses any astronomical signal that might be present in an individual reference star, and any residual variation is then dominated by systematics. Since

[1] http://keplergo.arc.nasa.gov/ContributedSoftwareKepcotrend.shtml.

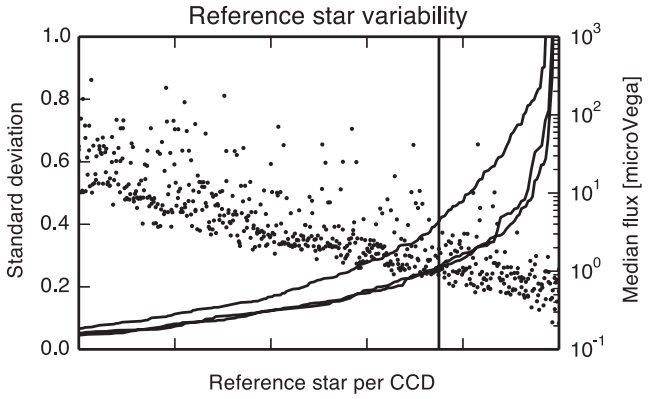

Figure 2. Flux variability (lines, left axis) and median flux (right axis, dots) for reference stars observed on the three different CCDs. The vertical line denotes the 75 per cent cut-off we chose for selecting quiet reference stars, only stars to the left are used in consequent de-correlation. While CCD 221 and 227 have similar variability roll-off, the upper solid line for CCD 228 indicates this CCD has noisier data. See the text for details.

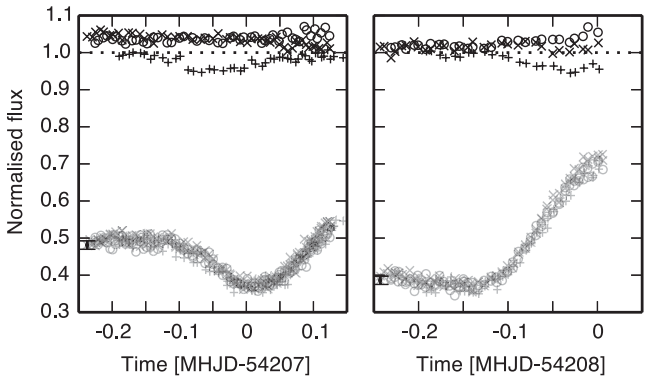

Figure 3. Comparison of de-correlation vector (top, black) and cleaned up light curve (bottom, grey) for nights MHJD 54 207 (left) and 54 208 (right). The three different CCDs are plotted with different symbols (◯, ×, and +), the de-correlation vector only shows every third data point for clarity. The de-correlation vectors for different CCDs differ significantly and indicate the different behaviour for each CCD. Without the de-correlation, this difference would result in a larger spread in the final light-curve data when combining data from different CCDs.

these stars are close to the target star, they are along nearly identical lines of sight through the atmosphere and camera optics, and so sample similar optical conditions. Additionally, these stars are close together on the CCD surface, such that they sample similar vignetting and electronic noise in the data.

Finally, to normalize the flux and allow inter-CCD comparison, we normalized the J1407 light curve by a linear fit for each CCD individually, excluding the eclipse window during MHJD 54 180–54 250. Through this de-correlation process, the photometry from the different CCDs now shows significantly less scatter (see Fig. 3). The result is shown in Fig. 4, where the flux from different CCDs are plotted against each other.

2.2 Stellar variability de-trending

After successfully de-correlating the signal from the systematics, we then remove the stellar variability. Mamajek et al. (2012) find that the J1407 light curve shows a variability of approximately 3.21 d in the SuperWASP data, as expected from rotational modulation of star spots and a young star of ∼16 Myr. Since this variability is independent of the eclipse signal, removing this signal is required for subsequent analysis.

First, we investigate the stellar variability for each of the three seasons, 2006, 2007 and 2008, where in 2007 we have only used the out-of-eclipse part of the light curve. We use phase dispersion minimization (Stellingwerf 1978) with a variable-period sinusoid as a model to allow for gradual change in the rotational period, given by

$$F_{\rm model} = A\ \sin(2\pi t/P(t) - \varphi_0) + F_0 \qquad (5)$$

with A the amplitude, t time, φ_0 the phase at $t = 0$, F_0 a flux offset of roughly one and $P(t)$ the linearly variable period, given by

$$P(t) = P_0 + \dot{P}t, \qquad (6)$$

where P_0 is the nominal period and $\dot{P}$ the time-derivative of the period. This model is fitted to the data using the Nelder–Mead fitting algorithm (Nelder & Mead 1965). Our analysis shows that the best-fitting periods and their amplitudes differ significantly from year to year (see Table 1). Furthermore, the amplitude of the variability is significantly less during the eclipse year 2007 than in the other years. We attribute the difference in observed rotational periods due to the change in the mean latitudinal position of star spots on the surface of J1407 and the differential rotation of the stellar atmosphere.

Initially, we fit the variability for the 2006 and 2008 data with a constant period and interpolated this to the 2007 data. However, this interpolated fit mismatches the 2007 data in both phase and amplitude, it appears the period is not constant enough for such interpolation. To mitigate this, we fit the stellar variability using the light curve just before and after the eclipse in 2007, i.e. before MHJD 54 197 and after 54 255 where we verified by eye that little to no eclipse signal is present, by plotting the wrapped light curve and increasing the window size until a suitable window was found. Although additionally fitting the 2006 and 2008 data better constrains this variability, this requires modelling of stellar variability outside the scope of this paper.

For the out of eclipse 2007 data, we find a period of 3.2011(2) d. The phase folded light curve for this stellar variability period is shown in Fig. 5. We de-trend the 2007 signal of interest by dividing the light curve by the normalized, best-fitting, variable-period sinusoid as to remove the stellar variability.

The de-correlated and de-trended light curve for 2007 is depicted in Fig. 6, the top panel shows the whole year while the bottom panel shows 25 d around the approximate eclipse mid-point MHJD 54 222. Ingress and egress show a similar trend of linearly decreasing opacity away from the eclipse mid-point, but the nightly structure is very different from night to night.

3 REVISED STELLAR PARAMETERS

Mamajek et al. (2012) presented estimated stellar parameters for J1407. Here, we present updated stellar parameters based on slightly revised astrometry and assumed intrinsic stellar colours and temperature.

Using the revised proper motion for J1407 from the UCAC4 catalogue (UCAC4 252-062736; Zacharias et al. 2013) and the space motion and convergent point solution for the Upper Centaurus–Lupus (UCL) subgroup from Chen et al. (2011), we estimate a revised (predicted) kinematic distance of 133 ±12 pc (ϖ = 7.49 ± 0.65 mas). This is consistent with the mean distance to the UCL subgroup from de Zeeuw et al. (1999): 140 pc.

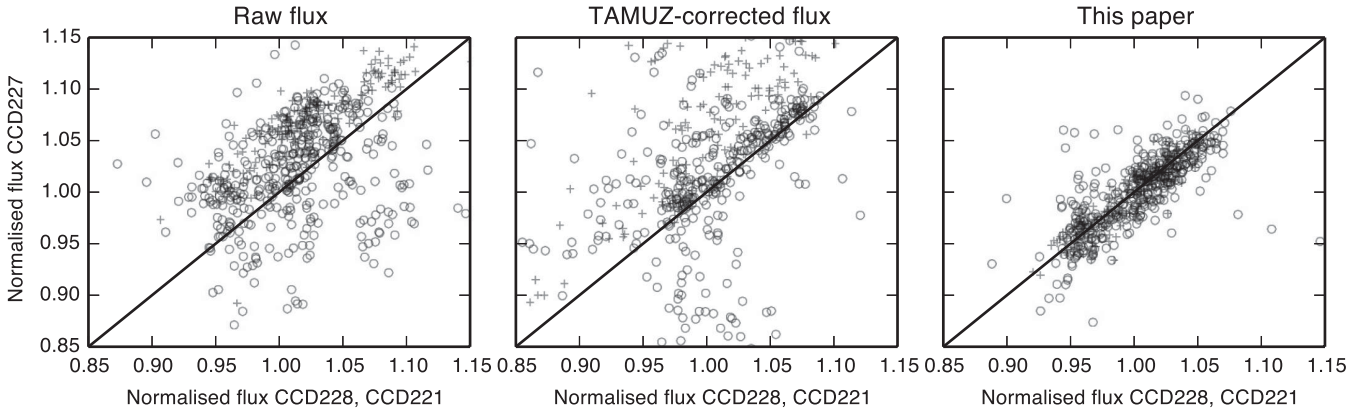

Figure 4. Hourly-binned flux from CCDs 221, 227, 228 plotted against each other (CCD227–CCD228: open circles, CCD227–CCD221: plus signs). The raw flux (FLUX) shows an offset between the CCDs as well as a significant scatter (Pearson's correlation coefficient $\rho = 0.49$), while the automatically reduced flux (TAMFLUX) is more consistent between different CCDs but still shows a large spread between the data ($\rho = 0.54$). The manually de-correlated flux shows no offset and significantly reduced scatter, indicating consistency between the three different CCDs ($\rho = 0.81$).

Table 1. Measured period (P) and period variability ($\dot{P}$) for J1407 in three years of SuperWASP data. The variability expresses the change of the period throughout each year as found by the phase dispersion minimization analysis described in the text.

Season	P (d)	$\dot{P}$ (sd^{-1})	A (per cent)
2006	3.2183(4)	22(2)	4.98(3)
2007	3.2011(2)	31(1)	3.57(2)
2008	3.2066(3)	0.8(6)	5.00(2)

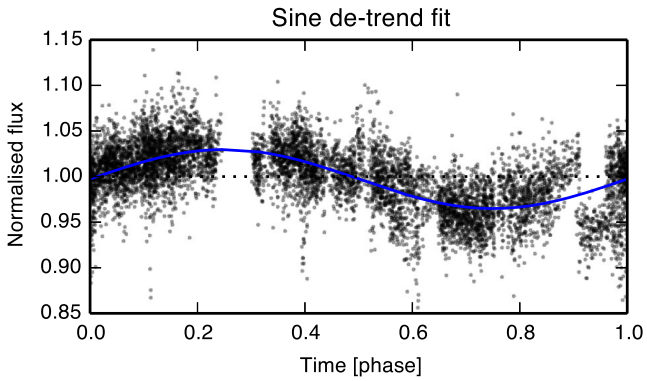

Figure 5. Normalized phase-folded SuperWASP flux for non-eclipse 2007 data with period $P = 3.2011(2)$ d showing the stellar variability. The solid line is a best-fitting sinusoid with variable period as described in equation (5).

Pecaut & Mamajek (2013) presented a revised sequence of intrinsic optical–infrared colours, effective temperature ($T_{\rm eff}$), and bolometric corrections as a function of spectral type for pre-main-sequence (pre-MS) stars. Adopting the spectral type of K5±1 from Mamajek et al. (2012), and the intrinsic properties of K5 pre-MS stars from Pecaut & Mamajek (2013), we estimate slightly revised stellar parameters: $T_{\rm eff} = 4140^{+190}_{-120}$ K and BC$_J \simeq 1.58 \pm 0.06$ mag. Using the revised intrinsic colours for K5 pre-MS stars, and the $BVJHK_s$ photometry for J1407 compiled in Mamajek et al. (2012), we estimate that the star is statistically consistent with being unreddened, but adopt extinction $A_J = 0.02 \pm 0.02$ ($A_V = 0.06 \pm 0.06$ mag). Combining the revised extinction, parallax and bolometric magnitude with the 2MASS J magnitude, we estimate the following parameters: $f_{\rm bol} = (6.09 \pm 0.38) \times 10^{-13}$ W m^{-2}, $m_{\rm bol} = 11.56 \pm 0.07$ mag, $M_{\rm bol} = 5.93 \pm 0.20$ mag, $\log(L/{\rm L}_\odot) = -0.47 \pm 0.08$ dex. The slight change to the adopted $T_{\rm eff}$, and negligible change to the luminosity, shifts the stellar radius slightly: 1.13 ± 0.14 R$_\odot$. In Table 2, we summarize the inferred isochronal ages and masses using grids of pre-MS modern evolutionary tracks and isochrones. The median mass (∼0.9 M$_\odot$) has changed negligibly; however, the cooler $T_{\rm eff}$ has moved the star from the radiative track to the Hayashi track, and produced correspondingly younger isochronal ages (∼10 ± 3 Myr). The isochronal ages of pre-MS K stars appear to be underestimated by nearly a factor of 2 compared to ages derived from the main-sequence turn-off, main-sequence turn-on and Li depletion boundary ages (cf. Pecaut, Mamajek & Bubar 2012; Bell et al. 2013; Soderblom et al. 2014). We continue to adopt the mean UCL age from Pecaut et al. (2012, , ∼16 Myr) as representative for J1407, but note that an age somewhere in the range of ∼5–20 Myr is possible. We adopt a mass of 0.9 ± 0.1 M$_\odot$ based on the HR diagram position of J1407, noting that four of the five sets of pre-MS evolutionary tracks lead to inferred masses closely bracketing ∼0.9 M$_\odot$. However, we note that if the inferred pre-MS isochronal ages may be in error by nearly a factor of ∼2, then the true masses may be systematically off by tens of per cent as well (see e.g. Hillenbrand & White 2004). At this point, we are not in a position to be able to quantify the magnitude of any potential systematic error in mass due to problems with the evolutionary tracks themselves.

In summary, the most significant change to the adopted parameters for J1407 is that the estimate radius is about 18 per cent larger compared to Mamajek et al. (2012). We adopt these new values as compiled in Table 3 in the following sections.

4 RING MODEL

After successfully removing instrument systematics and stellar variability, we use the improved photometry to constrain the geometrical parameters of this system by modelling the changes in intensity due to the passage of rings across the disc of the star. By measuring the slope in the light curve and assuming a diameter for the star, we can derive a lower limit to the speed at which the occulting object is moving.

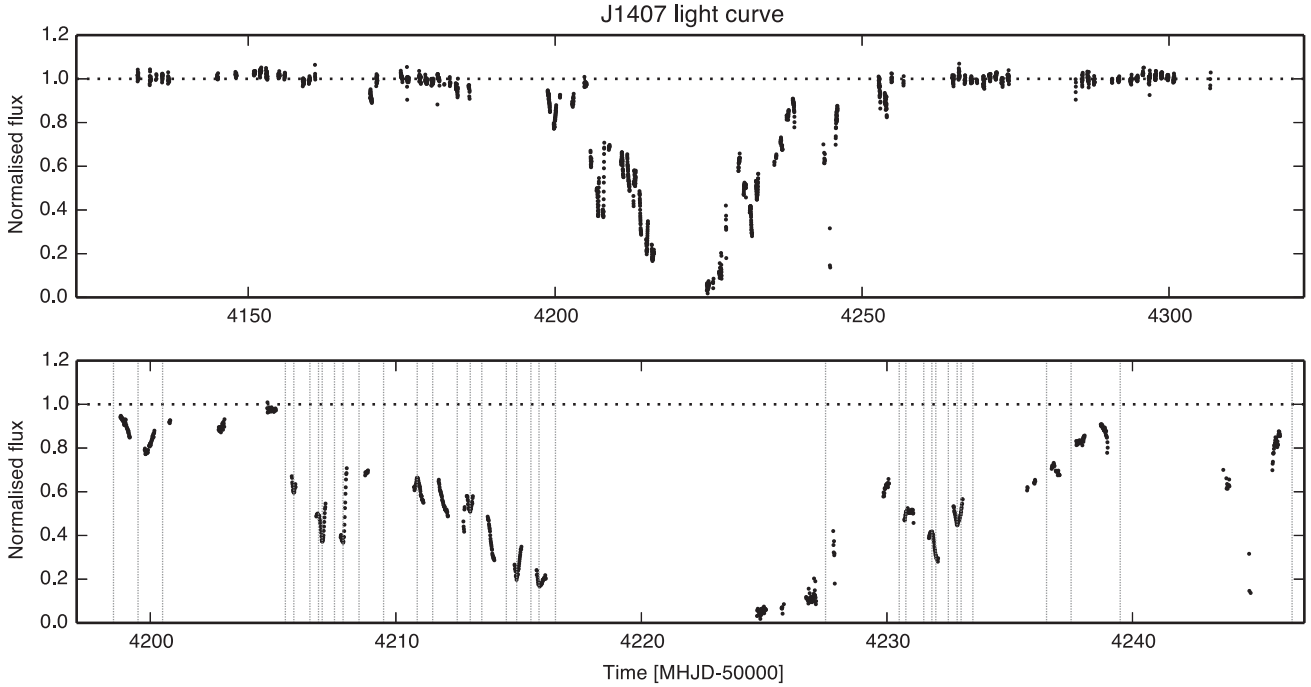

Figure 6. J1407 eclipse light curve as recorded by SuperWASP in 2007, corrected for systematics and stellar variability, binned in 15 min bins for clarity. Data are taken during the local night, daytime shows up as gaps. The eclipse mid-point is at approximately MHJD 54 222 and lasts at least 54 d with roughly symmetrical ingress and egress but asymmetry in the nightly variation. Top: overview of all of 2007. Bottom: zoom in on fine-structure during eclipse, with inflection points marked with vertical dotted lines.

Table 2. Isochronal age and mass estimates for J1407.

(1) Tracks –	(2) Age (Myr)	(3) Mass ($M_\odot$)
Baraffe et al. (1998)	10	0.90
Siess, Dufour & Forestini (2000)	12	0.88
Yi, Kim & Demarque (2003)	5	0.68
Dotter et al. (2008)	12	0.92
Paxton et al. (2011)[1]	9	0.87

Evolutionary tracks and isochrones were generated using the MESA evolutionary code (Paxton et al. 2011), adopting the protosolar abundances from Asplund et al. (2009, Strumpf, private communication).

Table 3. Revised stellar parameters.

(1) Property	(2) Value	(3) Ref.
α(J2000)	14:07:47.929	1
δ(J2000)	−39:45:42.75	1
μ_α	-24.3 ± 1.7 mas yr^{-1}	1
μ_δ	-19.4 ± 2.0 mas yr^{-1}	1
A_J	0.02 ± 0.02 mag	2
A_V	0.06 ± 0.06 mag	2
Dist	133 ± 12 pc	2
$T_{\rm eff}$	4140^{+190}_{-120} K	2
log ($L/L_\odot$)	-0.47 ± 0.08 dex	2
Age	∼16 Myr	3
Mass	0.9 ± 0.1 $M_\odot$	2

References: (1) Zacharias et al. (2013), (2) this paper, (3) adopted UCL age from Pecaut et al. (2012), see the discussion in text.

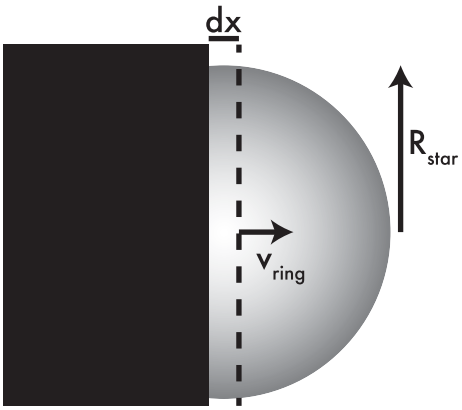

Figure 7. Eclipse geometry for an opaque ring crossing the star. In this scenario, no material is in front of the star before the ring arrives.

We model the eclipse geometry by assuming that an optically thick ring moves in front of the stellar disc. The stellar disc is approximated with a limb darkening model from Claret & Bloemen (2011). We assume that the ring is circular and azimuthally symmetric around J1407b, that the diameter of the ring is much larger than the diameter of the star so that the edge of the ring can be approximated as a straight line and that the edge of the ring is perpendicular to its direction of motion, as seen in Fig. 7. The observed light-curve slope dL/dt is given by the rate at which the surface of the star is eclipsed, multiplied with the mean intensity of the star in the eclipsed area. Below, we calculate light-curve slopes for a limb-darkened star. These approximations then present a lower limit for the relative velocity of the ring system – if the ring edge is not perpendicular to the direction of motion, then the ring velocity will be higher for a given dL/dt.

For our analysis, we use a linear limb-darkening law from Claret & Bloemen (2011):

$$I(\mu) = 1 - u(1-\mu), \tag{7}$$

with u being the limb-darkening coefficient, $\mu = \cos(\gamma)$, where γ is the angle between the line of sight and the surface normal. For stars such as J1407 ($T_{\rm eff} \sim 4500$ K, $\log g \sim 4.4$, [Fe/H] ~ 0), Claret & Bloemen (2011) find limb-darkening coefficient $u = 0.8(5)$ in the SuperWASP band. We rewrite μ as linear coordinate $r = \sqrt{1-\mu^2}$ from 0 at the centre of the disc to 1 at the limb to yield:

$$I(r) = 1 - u(1 - \sqrt{1-r^2}). \tag{8}$$

The flux in a small vertical strip of width dx at the centre of the stellar disc is then given by

$$\begin{aligned} F_{\rm strip} &= {\rm d}x \int_{-R}^{R} I(r/R)\,{\rm d}r \\ &= {\rm d}x\, 2\,R \left(1 - u + \frac{\pi u}{4}\right), \end{aligned} \tag{9}$$

while the total flux is given by

$$\begin{aligned} F_{\rm total} &= \int_0^R 2\pi r\, I(r/R)\,{\rm d}r \\ &= \frac{1}{6} R^2 \pi (6 - 2u), \end{aligned} \tag{10}$$

with R the stellar radius. The maximum light-curve slope is then given by the ratio of these, divided by the time dt it takes to cross distance dx, multiplied by the total stellar luminosity

$$\left(\frac{{\rm d}L}{{\rm d}t}\right)_{\rm max} = L_\star \frac{F_{\rm strip}}{F_{\rm total}} \frac{1}{{\rm d}t}. \tag{11}$$

We can rewrite this to obtain the implied speed for a given slope as

$$\begin{aligned} \left(\frac{{\rm d}x}{{\rm d}t}\right)_{\rm min} &= \dot{L}\, R\, \pi \frac{2u - 6}{12 - 12u + 3\pi u} \\ &\approx 13\ {\rm km\,s^{-1}} \left(\frac{\dot{L}}{L_\star\,{\rm d}^{-1}}\right) \left(\frac{R}{1.13\ {\rm R}_\odot}\right), \end{aligned} \tag{12}$$

where $v = {\rm d}x/{\rm d}t$ is the speed of the ring with respect to the star.

We now assume that J1407b is in a circular *Kepler* orbit around the central star with velocity v and semimajor axis a:

$$\begin{aligned} a &= G\,M/v^2 \\ &\approx 8.0\,{\rm au} \left(\frac{M}{0.9\ {\rm M}_\odot}\right) \left(\frac{v}{10\ {\rm km\,s^{-1}}}\right)^{-2}, \end{aligned} \tag{13}$$

and a disc diameter of

$$\begin{aligned} r_d &= v\, t_{\rm eclipse}/2 \\ &\approx 0.16\,{\rm au} \left(\frac{t_{\rm eclipse}}{54\ {\rm d}}\right) \left(\frac{v}{10\ {\rm km\,s^{-1}}}\right). \end{aligned} \tag{14}$$

Equation (14) is equivalent to equation 10 in Mamajek et al. (2012), although the authors missed a factor π in their equation. We can express the radius of the disc as a fraction of the Hill radius $r_{\rm H} \equiv a(\mu/3)^{1/3}$, with $\mu = m_2/(m_1 + m_2)$ as

$$\begin{aligned} \frac{r_d}{r_{\rm H}} \equiv \xi &= t_{\rm eclipse}\, v\, \frac{3^{1/3}}{a\,\mu^{1/3}} \\ &= 0.28 \left(\frac{t_{\rm eclipse}}{54\ {\rm d}}\right) \left(\frac{v}{10\ {\rm km\,s^{-1}}}\right)^3 \left(\frac{M}{0.9\ {\rm M}_\odot}\right)^{-2/3} \left(\frac{m_2}{{\rm M_J}}\right)^{-1/3}. \end{aligned} \tag{15}$$

To measure the light-curve slope for J1407, we fit straight lines to manually selected windows with constant slope. An overview of the light curve is shown in Fig. 8, where straight line fits are plotted over the data. The top panel shows the light curve during the eclipse and each panel below shows one night of data. We plot the measured light-curve slopes in Fig. 9.

5 RESULTS

A wealth of fine structure becomes visible in the light curve (Figs 6 and 8). By de-correlating against reference stars, we ensure these are not randomly occurring systematic effects, but are due to J1407. Removing the stellar variability further improves the photometry.

The light curve shows strong slopes of up to 3 $L_\star\,{\rm d}^{-1}$ (Table 5), which means that the eclipsing agent must have a speed such that the star is occulted in roughly 1/3 of a day. Furthermore, we find a myriad of fine structures in the light curve, with at least 24 inflection points on ingress, and 16 on egress (see Table 4 and Fig. 8), and changes of at 15 per cent or more in flux in six nights. Some inflection points are directly observed in the nightly data, whilst others are implied by a mismatch in photometric observations between consecutive observation windows, implying an unseen change in light-curve slope. These inflection points indicate the presence of at least 24 different rings in the J1407b system.

Given the light-curve slopes we measure and an estimate of the diameter of the star, we can compute the physical speed and diameter of the ring system. Using $R = 1.13(14)$ R$_\odot$, $M = 0.9(1)$ M$_\odot$ (this paper), $t_{\rm eclipse} = 54$ d (Mamajek et al. 2012) and $u = 0.8(5)$ (Claret & Bloemen 2011) gives the results shown in Fig. 9. The error bars are dominated by the 16 per cent error in the radius, an improved estimate for this would better constrain the disc parameters.

Most nights have $<15\,{\rm km\,s^{-1}}$ occultation speeds, but two nights during ingress have exceptionally high speeds. These slopes are 1.7 and 3.0 $L_\star\,{\rm d}^{-1}$, which correspond to 22(3) km s^{-1} to 38(5) km s^{-1}, respectively. While the first night is compatible with the $21.7\,{\rm km\,s^{-1}}$ upper limit found by Mamajek et al. (2012), the second night is not. Additionally, the highest speeds combined with the 54 d eclipse duration yield an outer-ring disc radius of 0.3 and 0.6 au, respectively. While part of this slopes could have be introduced by errors in the de-correlation or de-trending, this is not the case here. Fig. 3 shows two nights with steep light-curve changes alongside the de-correlation vector, for which no significant change is observed. Additionally, the 3.2 d, 4 per cent sinusoid used for de-trending has a maximum slope of 0.08 $L_\star\,{\rm d}^{-1}$, such that even if the de-trending were exactly out of phase, the majority of the slope would still be real.

Furthermore, we observe significant change in slopes on the time-scale of hours in the data, for example during nights -16, -15, -14, -11, 10, and 11 in Fig. 8, showing inflection points where the slope changes. This ratio of the variability time-scale of an hour over half the eclipse duration of 54 d implies an aspect ratio of the disc of $h/r \approx 0.0015$, confirming earlier findings by Mamajek et al. (2012).

6 DISCUSSION

The minimum speeds derived only from the light-curve slopes, stellar radius and limb darkening are incompatible with both the minimum period of 2.3 yr found by Mamajek et al. (2012), in spite of the large uncertainties on stellar properties. Also using the stellar mass and a secondary mass upper limit of 50 $M_{\rm J}$ based on sparse aperture mask imaging at K_s on the VLT (Kenworthy, private communication), the disc is also overfilling the Hill radius for the largest

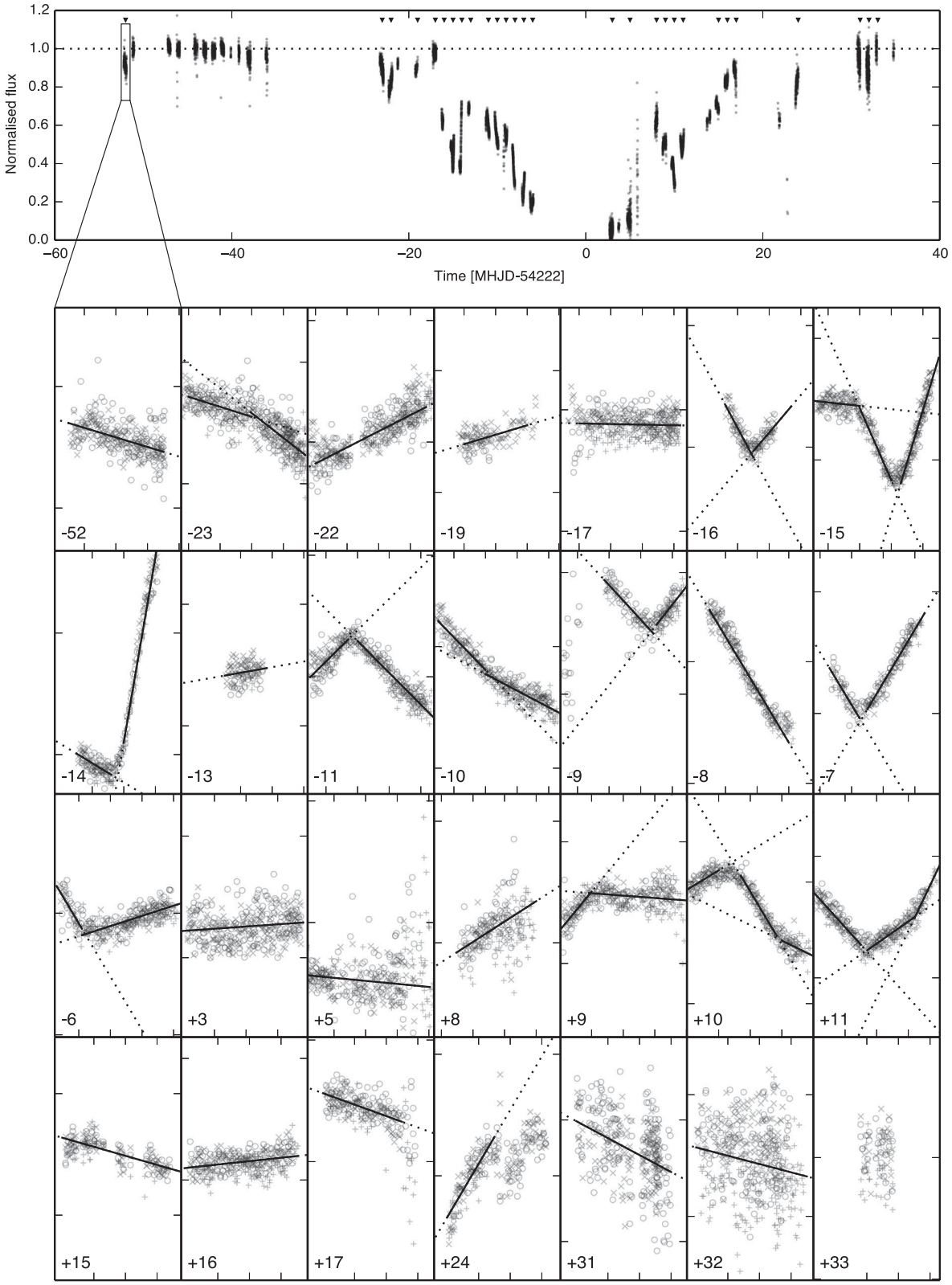

Figure 8. Detailed plot of the J1407 light curve during the eclipse. Top: overview of the light curve. Bottom: nightly light curve for 28 nights during the eclipse, indicated in the upper panel by triangles. The data from the different CCDs are plotted with different symbols, 221: ◯, 227: ×, and 228: +. The straight line fits are plotted over the data, solid lines are inside the window used for the fit, dotted line are extrapolated. The y-ticks are spaced at 0.2 au (as in the top panel) and x-ticks at 0.1 d.

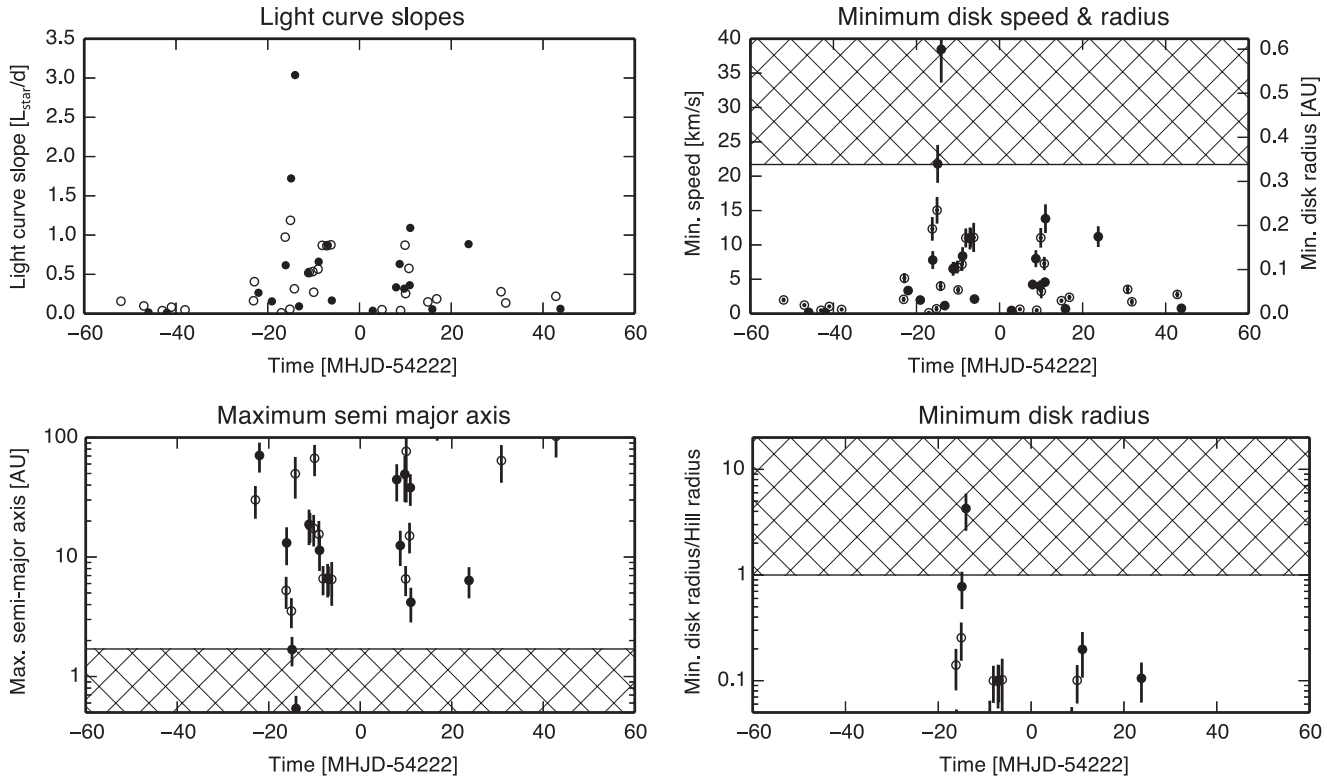

Figure 9. Light-curve slopes and derived system parameters for circular orbits. Top left: light-curve slopes during the eclipse, top right: orbital disc speeds and disc radii, bottom left: semimajor axes, bottom right: disc radius over the Hill radius, assuming $m_2 = 50\ M_J$. The eclipse mid-point is approximately at MHJD 54 222. Filled circles are positive slopes (i.e. increasing flux), open circles represent negative slopes. The hatched area represents data incompatible with the minimum period of 2.3 yr (lower left and top right) or data that predict disks larger than the Hill radius (lower right).

minimum speed. Here, we briefly consider two scenarios that could mitigate these problems, the first being an elliptical orbit and the second substructure in the rings.

6.1 Ellipsoidal orbits for J1407b

An ellipsoidal orbit would allow for larger periastron speeds and explain the anomalous velocities implied in the data; however, these are not fast enough to explain the observations. For a *Kepler* orbit with period P and ellipticity e, we compute the maximum speed at periastron

$$v_{\rm max} = \left(\frac{2\pi G M}{P}\right)^{1/3} \left(\frac{1+e}{1-e}\right)^{1/2}. \quad (16)$$

These speeds are plotted as dashed lines in Fig. 10. This maximum speed combined with the eclipse duration of 54 d gives a disc radius. Additionally, for a planetary mass m_2, we can compute the Hill radius at the periastron

$$R_{\rm Hill} = \left(\frac{m_2 G P^2}{12\pi^2}\right)^{1/3} (1-e). \quad (17)$$

We then solve $R_{\rm disc} = R_{\rm Hill}$ using equations (14) and (17) for m_2, plotted as solid lines in Fig. 10. Since the secondary mass is less than 50 M_J, ellipticity alone cannot explain the speeds derived from the observed slopes.

6.2 Azimuthal structure in the rings

If there is non-radial structure in the ring, e.g. a bar or clumps in the ring, this could give rise to an increased slope dL/dt. Such radial structures ('spokes') have been observed in the B-rings of Saturn (Smith et al. 1982). With azimuthal density structures in the ring, these could vectorially add to the observed light-curve slope, as shown in Fig. 11. The night showing the highest light-curve slope is at approximately 14 d before the eclipse mid-point. Assuming $m_2 = 50\ M_J$ and $P = 3.5$ yr, this would give an orbital speed of the planet of $v_{\rm ring} = 19\ {\rm km\,s^{-1}}$ such that the ring distance would be at $19\ {\rm km\,s^{-1}} \times 14\ {\rm d} = 0.15$ au. For this radius, the ring would rotate at a speed of $v_{\rm clump} = 17\ {\rm km\,s^{-1}}$, which in total would yield a occulting speed of $36\ {\rm km\,s^{-1}}$, compatible with the observations.

6.3 Forward scattering

A third option is that the observed slope is a combination of the slope from a ring eclipsing edge added with an additional slope due to forward scattering from the particles making up the ring wall. Such forward scattering is seen and modelled in Fomalhaut's debris disc (Kalas, Graham & Clampin 2005) and in the light curve produced by a disintegrating exoplanet KIC 12557548 b (Brogi et al. 2012; Rappaport et al. 2012). Since we do not know the thickness of the disc and a unique ring geometry, we do not carry out the modelling in this paper.

7 CONCLUSIONS

We have reduced the SuperWASP extracted photometric flux data for J1407 using an ensemble of photometrically quiet nearby reference stars to remove systematic effect in the data, and de-trended for stellar variability, showing an improvement over the raw flux as

Table 4. Inflection points in the J1407 light-curve slope indicative of opacity change. Each inflection point indicates a change in slope, which in turn implies change in opacity, and thus a new ring beginning to eclipse the star. Time is shown in MHJD−54 222. The numbers marked with an asterisk are approximate, indicating the presence of an inflexion point during daylight hours but whose presence is implied by the light curves in adjacent photometric measurements. See also Fig. 8.

Inflection point (d)	
Ingress	Egress
−5.5*	5.5*
−6.17	8.5*
−6.5*	8.77
−7.08	9.5*
−7.5*	9.83
−8.5*	9.99
−8.97	10.5*
−9.5*	10.86
−10.5*	11.02
−11.13	11.5*
−12.5*	14.5*
−13.5*	15.5*
−14.15	17.5*
−14.5*	24.5*
−15	31.5*
−15.15	32.5*
−15.5*	–
−16.155	–
−16.5*	–
−21.5*	–
−22.5*	–
−23.5*	–
−51.5*	–
−52.5*	–

Table 5. Measured light-curve slopes greater than $0.1\,\mathrm{d}^{-1}$ and derived circular orbital speed. Time is shown in MHJD−54 222.

Time (d)	Slope (d^{-1})	Speed ($\mathrm{km\,s}^{-1}$)
−52.00	−0.16(2)	−2.0(3)
−23.10	−0.16(2)	−2.1(4)
−22.92	−0.41(3)	−5.2(7)
−22.02	0.270(9)	3.4(4)
−19.10	0.16(3)	2.0(4)
−16.19	−0.97(6)	−12(2)
−16.09	0.62(7)	8(1)
−15.05	−1.19(4)	−15(2)
−14.91	1.72(4)	22(3)
−14.19	−0.32(4)	−4.0(7)
−14.04	3.04(6)	38(5)
−11.19	0.52(5)	7(1)
−10.97	−0.52(1)	−6.6(8)
−10.18	−0.54(3)	−6.8(9)
−9.98	−0.27(1)	−3.5(5)
−9.04	−0.57(3)	−7(1)
−8.90	0.66(6)	8(1)
−8.12	−0.87(2)	−11(1)
−7.12	−0.86(7)	−11(2)
−6.96	0.87(2)	11(1)
−6.23	−0.9(1)	−11(2)
−6.04	0.17(1)	2.1(3)
7.97	0.33(4)	4.2(7)
8.75	0.63(6)	8(1)
9.75	0.32(5)	4.0(8)
9.93	−0.87(3)	−11(1)
10.05	−0.26(7)	−3(1)
10.77	−0.58(3)	−7(1)
10.94	0.36(2)	4.6(6)
11.06	1.09(9)	14(2)
14.90	−0.15(1)	−1.9(3)
16.82	−0.19(2)	−2.4(4)
23.77	0.88(5)	11(2)
30.85	−0.28(3)	−3.5(6)
31.88	−0.14(3)	−1.7(4)
42.80	−0.22(2)	−2.8(4)

well as the automatically reduced flux pipeline outputs. We find a periodicity of approximately 3.2 d for the different observation seasons, with significant differences between the seasons. We attribute the difference in observed rotational periods due to the change in the mean latitudinal position of star spots on the surface of J1407 and the differential rotation of the stellar atmosphere.

With the newly reduced photometry, we have investigated the nightly structure in the light curve during the eclipse and find strong slopes of up to $\sim 3 L_\star\,\mathrm{d}^{-1}$. Furthermore, we find a myriad of fine structures in the light curve, which we explain with the eclipse of a ring system orbiting around J1407b and we identify at least 24 different rings. Given that for a disc alone, this structure would be radially smeared out by internal disc interactions on short dynamical time-scales, this is indicative of the presence of shepherding exomoons.

Using a simple model of a limb-darkened star, we calculate the minimum orbital speed implied by the observed light-curve slopes. We find that these minimum speeds are incompatible with the analysis by Mamajek et al. (2012) who find a minimum period of 2.3 yr. Although an elliptic orbit could alleviate this problem to some extent, it cannot completely explain the largest slopes in the light curve. We propose substructure in the rings in forms of clumps (appearing as 'spokes') as a plausible explanation for the observed slopes.

Further observations to constrain the orbital period and mass of J1407 are required to better understand this system. Atacama Large Millimeter Array (ALMA) is capable of directly detecting rings down to $0.8\,M_{\mathrm{moon}}$ masses (as estimated by Mamajek et al. 2012) in a few hours, and its spatial resolution would enable a unique confirmation of the bound orbit of J1407b around J1407. Several small telescopes are currently monitoring for the beginning of the next eclipse, and an intensive monitoring campaign to cover the duration of the 60 d eclipse would give an unprecedented opportunity for the resolved study of a circumplanetary ring system outside our Solar system. Spectroscopy over a broad range of wavelengths can characterize the density and composition of the rings, providing new insight into their formation and origins. The high rotation of the star, combined with high-resolution spectroscopy, leads to the exciting possibility of observing the Rossiter–McLaughlin effect (Rossiter 1924; McLaughlin 1924) as the ring edges eclipse the stellar disc and a subsequent increase in spatial resolution in the ring structure. Initial modelling efforts by our group show that a continuous time coverage using multiple telescopes spread over different latitudes will be essential in constraining the system and determining the ring geometry present there.

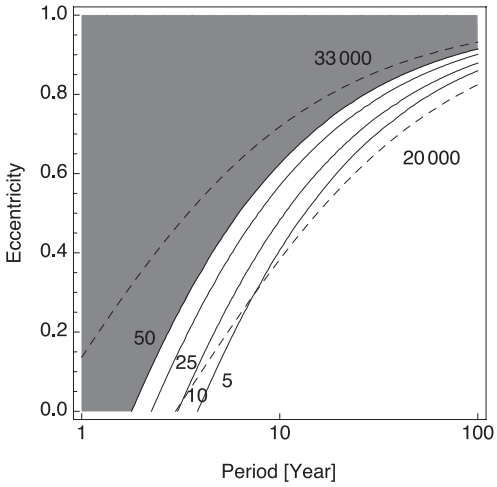

Figure 10. Secondary mass for $R_{\rm disc} = R_{\rm Hill}$ in M_J (solid lines) and maximum orbital speed in m s^{-1} (dashed lines), both as function of period and eccentricity. For a given secondary mass (solid line), the area below the line is allowed: in those cases the eccentricity is less, giving a larger minimum separation and thus a larger Hill radius, thus fitting in the disc. For a given speed (dashed line), the area above the curve is allowed: in those cases the eccentricity is higher and thus the maximum speed is larger. For the highest speed calculated from the light-curve slopes, there is no region compatible with stable rings given that the secondary mass is limited to 50 M_J. The second highest speed could be explained by ellipticity with a <3 yr orbit, or with a secondary mass of 25 M_J above that.

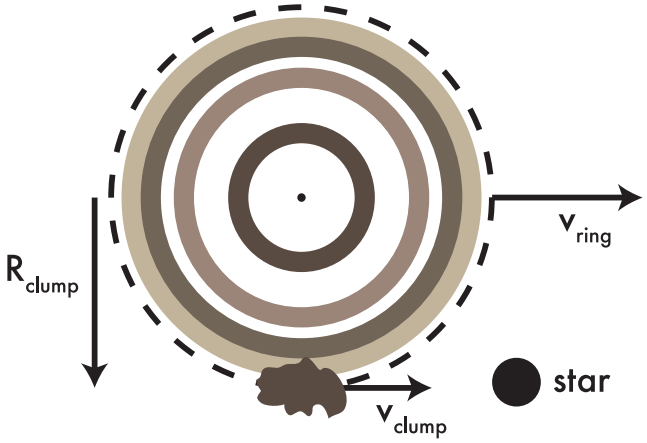

Figure 11. Geometry of a clump in a circular orbit around J1407b eclipsing the star. In this case, the speed of the disc with respect to the star ($v_{\rm ring}$) vectorially adds to the speed of the clump in the ring ($v_{\rm clump}$). Outer rings are not shown for clarity.

ACKNOWLEDGEMENTS

The authors thank the referee Keivan Stassun for providing critical and valuable feedback. The WASP project is funded and operated by Queen's University Belfast, the Universities of Keele, St Andrews and Leicester, the Open University, the Isaac Newton Group, the Instituto de Astrofísica de Canarias, the South African Astronomical Observatory and by STFC. EEM acknowledges support from NSF grants AST-1008908 and AST-1313029. MAK acknowledges funding under the Marie Curie International Reintegration Grant 277116 submitted under the Call FP7-PEOPLE-2010-RG.

REFERENCES

Asplund M., Grevesse N., Sauval A. J., Scott P., 2009, ARA&A, 47, 481
Baraffe I., Chabrier G., Allard F., Hauschildt P. H., 1998, A&A, 337, 403
Bell C. P. M., Naylor T., Mayne N. J., Jeffries R. D., Littlefair S. P., 2013, MNRAS, 434, 806
Brogi M., Keller C. U., Ovelar D. J., Kenworthy M. A., de Kok R. J., Min M., Snellen I. A. G., 2012, A&A, 545, L5
Butters O. W. et al., 2010, A&A, 520, L10
Cameron A. C. et al., 2007, MNRAS, 375, 951
Chen C. H., Mamajek E. E., Bitner M. A., Pecaut M., Su K. Y. L., Weinberger A. J., 2011, ApJ, 738, 122
Claret A., Bloemen S., 2011, VizieR Online Data Catalog, 352, 99075
de Zeeuw P. T., Hoogerwerf R., de Bruijne J. H. J., Brown A. G. A., Blaauw A., 1999, AJ, 117
Dotter A., Chaboyer B., Jevremović D., Kostov V., Baron E., Ferguson J. W., 2008, ApJS, 178, 89
Fraquelli D., Thompson S. E., 2012, Technical Report, Kepler Archive Manual (KDMC-10008-004). Space Telescope Science Institute, Baltimore, MD
Guinan E. F., Dewarf L. E., 2002, in Tout C. A., van Hamme W., eds, ASP Conf. Proc. Vol. 279, Exotic Stars as Challenges to Evolution. Astron. Soc. Pac., San Francisco, p. 121
Hillenbrand L. A., White R. J., 2004, ApJ, 604, 741
Kalas P., Graham J. R., Clampin M., 2005, Nature, 435, 1067
Kane S. R., Cameron A. C., Horne K., James D., Lister T. A., Pollacco D. L., Street R. A., Tsapras Y., 2004, MNRAS, 353, 689
McLaughlin D. B., 1924, ApJ, 60, 22
Mamajek E. E., Quillen A. C., Pecaut M. J., Moolekamp F., Scott E. L., Kenworthy M. A., Cameron A. C., Parley N. R., 2012, AJ, 143, 72
Mikolajewski M., Graczyk D., 1999, MNRAS, 303, 521
Nelder J. A., Mead R., 1965, Comput. J., 7, 308
Norton A. J. et al., 2011, A&A, 528, A90
Paxton B., Bildsten L., Dotter A., Herwig F., Lesaffre P., Timmes F., 2011, ApJS, 192, 3
Pecaut M. J., Mamajek E. E., 2013, ApJS, 208, 9
Pecaut M. J., Mamajek E. E., Bubar E. J., 2012, ApJ, 746, 154
Pollacco D. L. et al., 2006, PASP, 118, 1407
Rappaport S. et al., 2012, ApJ, 752, 1
Rossiter R. A., 1924, ApJ, 60, 15
Siess L., Dufour E., Forestini M., 2000, A&A, 358, 593
Smith B. A. et al., 1982, Science, 215, 504
Soderblom D. R., Hillenbrand L. A., Jeffries R. D., Mamajek E. E., Naylor T., 2014, in Beuther H., Klessen R., Dullemond C., eds, Protostars and Planets VI. Univ. Arizona Press, Tucson, AZ, p. 83
Stellingwerf R. F., 1978, ApJ, 224, 953
Tamuz O., Mazeh T., Zucker S., 2005, MNRAS, 356, 1466
Yi S. K., Kim Y.-C., Demarque P., 2003, ApJS, 144, 259
Zacharias N., Finch C. T., Girard T. M., Henden A., Bartlett J. L., Monet D. G., Zacharias M. I., 2013, AJ, 145, 44

This paper has been typeset from a TEX/LATEX file prepared by the author.